Adaptive Sparse-binary Waveform Design for All-spectrum Channelization

George Sklivanitis[a], Panos P. Markopoulos[b], Stella N. Batalama[a], and Dimitris A. Pados[a]

[a]Department of Electrical Engineering, State University of New York at Buffalo, Buffalo, NY 14260, USA
[b]Department of Electrical and Microelectronic Engineering, Rochester Institute of Technology, Rochester NY 14623, USA

ABSTRACT

We introduce maximum-SINR, sparse-binary waveforms that modulate data information symbols over the entire continuum of the available/device-accessible spectrum. We present an optimal algorithm that designs the proposed waveforms by maximizing the signal-to-interference-plus-noise ratio (SINR) at the output of the maximum-SINR linear filter at the receiver. In addition, we propose a suboptimal, computationally-efficient algorithm. Simulation studies compare the proposed sparse-binary waveforms with their conventional non-sparse binary counterparts and demonstrate their superior SINR performance. The post-filtering SINR and bit-error rate (BER) improvements attained by the proposed waveforms are also experimentally verified in a software-defined radio testbed operating in multipath laboratory environment, in the presence of colored interference.

Keywords: All-spectrum, cognitive channelization, sparse, software-defined radio testbed, waveform design

1. INTRODUCTION

In recent years, binary-code waveforms attracted considerable attention in applications such as physical layer security,[1,2] data hiding,[3,4] steganography,[5,6] cognitive radio,[7–11] and underwater networking.[12] Recent cognitive radio underlay networking proposals[7–12] consider adaptive transmission power and binary-code waveform optimization for secondary users that co-exist in time and frequency with primary users. Transmission power and binary-code waveforms are cognitively optimized over the entire available/device-accessible spectrum to maximize the signal-to-interference-plus-noise ratio (SINR) of secondary links and, at the same time, guarantee quality-of-service (QoS) constraints for primary communication links.

In the context of overloaded code-division multiple-access (CDMA), recently proposed systems consider the design of non-orthogonal sparse code waveforms to enable effective co-channel separation of multiple users with low complexity. Related work[13] defines a specific group of sparse code sequences that enable near-optimal, multi-user detection using belief propagation (BP). Considerable spectral-efficiency improvements are demonstrated for small values of sparsity in a statistical-mechanics framework[14] for sparse CDMA. Under the assumption of additive-white-Gaussian noise (AWGN) channels, prior-work[15] on sparse CDMA presents a design technique for constructing low-density, sparse code sequences with favorable distance spectrum properties. Another proposal[16] considers conducting synthesis of low-density spreading sequences based on a trial-and-error search basis, while recent work[17] describes a multiplexing scheme that enjoys low-complexity reception due to sparse spreading.

Binary-code waveforms for dense spreading sets have been well studied in terms of total-squared correlation (TSC) bounds and optimal designs.[18] New bounds and optimal designs for minimum-TSC quaternary signature sets have also been derived.[19] Related work on binary-code waveform design for sparse spreading is very limited.

Further author information: (Send correspondence to D.A.P.)
G.S.: E-mail: gsklivan@buffalo.edu, Telephone: +1 (716) 361 2664
P.P.M.: E-mail: panos@rit.edu, Telephone: +1 (585) 475-7917
S.N.B.: E-mail: batalama@buffalo.edu, Telephone: +1 (716) 645-1147
D.A.P.: E-mail: pados@buffalo.edu, Telephone: +1 (716) 645-1150

Compressive Sensing VI: From Diverse Modalities to Big Data Analytics, edited by Fauzia Ahmad, Proc. of SPIE Vol. 10211, 102110B · © 2017 SPIE
CCC code: 0277-786X/17/$18 · doi: 10.1117/12.2262311

Recent work[20] considers quadrature amplitude modulation (QAM) and provides a framework for designing sparse spreading-code matrices with maximum minimum code distance.

In this paper, instead of static binary waveforms, we propose for the first time adaptive design of sparse-binary waveforms that maximize SINR at the output of the maximum-SINR linear filter at the receiver. We present both an optimal sparsity waveform design algorithm and a suboptimal computationally efficient one. Simulation studies and experiments on a software-defined radio (SDR) testbed demonstrate the superiority of the proposed method in terms of post-filtering SINR and bit-error rate (BER).

The rest of the paper is organized as follows. In Section 2, we introduce the system model. Section 3 presents receiver design considerations and Section 4 discusses the proposed sparse waveform design. Section 5 offers simulation studies, describes the SDR testbed, and presents experimental results that demonstrate the superior performance of the proposed sparse-binary waveforms. A few concluding remarks are drawn in Section 6.

2. SYSTEM MODEL

We consider a single-antenna all-spectrum user transmitting information symbols from a unit energy phase-shift keying (PSK) constellation $\mathcal{A}$ over a single-input single-output (SISO) flat-fading channel with M resolvable paths, in the presence of colored interference. Specifically, the user of interest transmits J symbols $b[i] \in \mathcal{A}, i = 0, \dots J-1$, at rate $1/T$, modulated by a waveform $d(t)$ of duration T. The transmitted signal takes the form

$$x(t) \triangleq \sqrt{E} \sum_{i=0}^{J-1} b[i] d(t - iT) e^{j(2\pi f_c t + \phi)} \tag{1}$$

where $E > 0$ denotes the transmitted energy per symbol, and ϕ is the carrier phase with carrier frequency f_c. The modulating waveform is of the form

$$d(t) \triangleq \sum_{l=0}^{L-1} s[l] g_{T_d}(t - lT_d) \tag{2}$$

where $\mathbf{s} \in \left\{ \pm \frac{1}{\sqrt{L}} \right\}^L$ is a length-L binary code, and $g_{T_d}(\cdot)$ is a square-root-raised-cosine (SRRC) pulse of duration T_d so that $T = LT_d$. The transmitted signal is considered to propagate over a Rayleigh multipath fading channel and experience colored interference and complex additive white Gaussian noise at the receiver. Multipath fading is modeled by a linear tapped-delay line with taps that are spaced at T_d intervals and are weighted by independent fading coefficients. Fading is modeled by multiplicative complex Gaussian random variables (Rayleigh distributed amplitude and uniformly distributed phase). The received signal, after carrier demodulation at $f_c + \Delta f$, can be written as

$$\begin{aligned} r(t) &\triangleq \sum_{m=0}^{M-1} \tilde{h}[m]\ x(t - mT_d) e^{-j2\pi \Delta f t} + i(t) + n(t) \\ &= \sqrt{E} \sum_{i=0}^{J-1} b[i] \sum_{m=0}^{M-1} \tilde{h}[m]\ d(t - iT - mT_d) e^{-j2\pi \Delta f t} + \tilde{n}(t), \end{aligned} \tag{3}$$

where Δf is the carrier-frequency offset (CFO) due to clock drift between the local oscillators of the transmitter and receiver and $\tilde{h}[m] \triangleq h[m] e^{-j(2\pi f_c m T_d - \phi)}$ denotes the complex baseband channel coefficients for the m-th path. $\{h[m]\}_{m=0}^{M-1}$ are independent zero-mean complex Gaussian random variables that model the fading phenomena and are assumed to remain constant over at least J symbol intervals. Colored interference and additive white Gaussian noise at the receiver are modeled by $i(t)$ and $n(t)$, which form the compound disturbance $\tilde{n}(t) \triangleq i(t) + n(t)$.

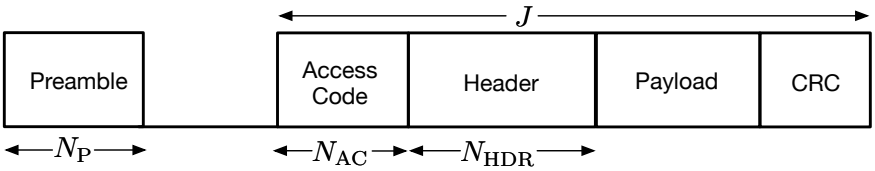

Figure 1. Frame structure. A length-N_{P} Barker sequence is used as preamble for frame detection. N_{AC} unmodulated access-code bits are used for CFO estimation and compensation, while N_{HDR} header symbols are used for time synchronization and channel estimation at the receiver.

3. RECEIVER DESIGN

In this section, we present receiver design considerations related to frame detection, CFO estimation and compensation, symbol-level time synchronization, channel estimation, maximum SINR filtering and symbol detection.

Let T_s and $I = \frac{T_d}{T_s}$ denote the sampling period and the number of samples per code-symbol, respectively. In view of (3), the k-th received sample from the analog-to-digital converter (ADC) at the SDR receiver can be written as

$$r[k] \triangleq r(kT_s) = \sqrt{E} \sum_{i=0}^{J-1} b[i] \sum_{m=0}^{M-1} \tilde{h}[m]\ d((k - iLI - mI)T_s) e^{-j2\pi\Delta f k T_s} + \tilde{n}(kT_s). \tag{4}$$

3.1 Frame detection

We consider that all-spectrum, frame-based, burst transmissions of symbols are preceded by length-N_{P} Barker sequences in the form of a preamble that is known a-priori at the receiver and is used for frame detection (see Fig. 1). The k-th received sample of the preamble sequence at the SDR receiver can be written as

$$r_p[k] \triangleq r_p(kT_s) = \sum_{m=0}^{M-1} \tilde{h}[m]\ x_p((k - mI)T_s) e^{-j2\pi\Delta f k T_s} + \tilde{n}(kT_s) \tag{5}$$

where $x_p(t) \triangleq \sqrt{E_p} \sum_{i=0}^{N_{\mathrm{P}}-1} b_p[i] g_{T_d}(t - iT_d)$ is the transmitted preamble sequence in baseband, $b_p[i] \in \{\pm 1\}, i = 0, \ldots, N_{\mathrm{P}} - 1$ are preamble symbols, and E_p is the transmitted energy per preamble symbol. Correlation of the received preamble sequence with the known preamble sequence at the receiver yields

$$R[k] \triangleq \sum_{n=0}^{N_{\mathrm{P}}-1} r_p[k]\ x_p^*[k + n]. \tag{6}$$

Barker sequences are selected due to their aperiodic autocorrelation characteristics.[21] More specifically, $R[k]$ will take its maximum value for $k = 0$ and low values for $k > 0$. The peak value at the output of the correlator will signify the beginning of the frame. The frame structure is summarized in Fig. 1.

3.2 Frequency synchronization

The samples of the received signal $r[k]$ are modulated by a CFO Δf with respect to the transmitted signal. CFO between different radios appears due to drifting oscillator frequencies of the transmitter and receiver. The first N_{AC} access-code bits of each frame are unmodulated (i.e. $b[i] = 1$, $i = 0, \ldots, N_{\mathrm{AC}} - 1$) which implies that the first N_{AC} replicas of the digital waveform $d(t)$ are also unmodulated. We exploit the pattern of the $N_{\mathrm{AC}} \cdot L \cdot I$ access-code training samples[9] to obtain a quality estimate $\widehat{\Delta f}$ as

$$\widehat{\Delta f} \triangleq \frac{1}{2\pi LI} \angle \sum_{i=0}^{(N_{\mathrm{AC}}-1)LI-1} r\,[i]\, r^*\,[i + LI]\,. \tag{7}$$

Then, the receiver compensates for the CFO in the acquired frame by applying $\widehat{\Delta f}$ to the k-th received sample as follows

$$y[k] \triangleq y(kT_s) = r[k]\exp(j2\pi\widehat{\Delta f}kT_s). \tag{8}$$

3.3 Symbol-level time synchronization

After discarding the first N_{AC} access-code bits, the frequency-synchronized received samples $y[k]$ are now ready for pulse-matched filtering and sampling at rate $1/T_d$ over the multipath extended period of $L+M-1$ code-symbols. However, there is a timing uncertainty regarding the sample $y[k]$ that corresponds to the the first header symbol (see Fig. 1). Symbol-level time synchronization is conducted by calculating and buffering all possible $(N_{\mathrm{HDR}}L)$-shifted crosscorrelation matrices

$$\mathbf{R}^{(l)} \triangleq \frac{1}{J'}\sum_{i=0}^{J'-1}\mathbf{y}_i^{(l)}\ \mathbf{y}_{\mathrm{HDR},i}^H, \quad l=0,\ldots,N_{\mathrm{HDR}}L-1 \tag{9}$$

where $J' = J - N_{\mathrm{AC}}$,

$$\mathbf{y}_i^{(l)} \triangleq \begin{bmatrix} y\left[(iL+l)I\right] \\ y\left[(iL+l+1)I\right] \\ \vdots \\ y\left[((i+1)L+M+l-2)I\right] \end{bmatrix}, \quad i=0,\ldots,J'-1, \tag{10}$$

$$\mathbf{y}_{\mathrm{HDR},i} \triangleq \begin{cases} \begin{bmatrix} b[N_{\mathrm{AC}}+i]\ s[0] & \ldots & b[N_{\mathrm{AC}}+i]\ s[L-1] \end{bmatrix}^T, & i=0,\ldots,N_{\mathrm{HDR}}-1 \\ \mathbf{0}_L^T, & i=N_{\mathrm{HDR}},\ldots,J'-1 \end{cases}, \tag{11}$$

and $\mathbf{0}_L$ is the all-zeros vector of length L. The beginning of the first header symbol is thus estimated as[9]

$$\hat{\tau}_0 \triangleq \underset{l\in\{0,\ldots,N_{\mathrm{HDR}}L-1\}}{\operatorname{argmax}} \|\mathbf{R}^{(l)}\|_F^2. \tag{12}$$

Next, we assume $M \le (L/2)+1$ and $T = LT_d >> T_m$, (where T_m is the multipath spread of the channel) so that the effect of inter-symbol interference (ISI) is negligible. The received data vector after pulse-matched filtering, symbol-level synchronization, and sampling at the code-symbol rate $1/T_d$, takes the form

$$\mathbf{y}_i \triangleq [\mathbf{y}]_{(\hat{\tau}_0+iL)I:I:(\hat{\tau}_0+L+M-2+iL)I}, \quad i=0,\ldots,J'-1 \tag{13}$$

which is equivalent to

$$\mathbf{y}_i = \sqrt{E}\mathbf{H}\mathbf{s}b[N_{\mathrm{AC}}+i] + \tilde{\mathbf{n}}_i \in \mathbb{C}^{L_M\times 1} \tag{14}$$

where $L_M = L+M-1$, $\mathbf{H}\in\mathbb{C}^{L_M\times L}$ is the multipath channel matrix and $\tilde{\mathbf{n}}_i \triangleq \mathbf{i}_i + \mathbf{n}_i$ where $\mathbf{i}_i \in \mathbb{C}^{L_M\times 1}$ is the colored interference vector with autocorrelation matrix $\mathbf{R}_{\mathbf{i}} \triangleq \mathbb{E}\{\mathbf{i}_i\mathbf{i}_i^H\} \in \mathbb{C}^{L_M\times L_M}$ and $\mathbf{n}_i \sim \mathcal{CN}(\mathbf{0}_{L_M}, \sigma^2\mathbf{I}_{L_M})$ is the additive white Gaussian noise vector. The multipath fading channel matrix between the transmitter and receiver can be written as

$$\mathbf{H} \triangleq \sum_{m=0}^{M-1}\tilde{h}[m]\begin{bmatrix} \mathbf{0}_{n\times L} \\ \mathbf{I}_{L\times L} \\ \mathbf{0}_{(M-n-1)\times L} \end{bmatrix} \in \mathbb{C}^{L_M\times L}. \tag{15}$$

In addition, for any general waveform $\mathbf{s}$ with $\|\mathbf{s}\|_2 = 1$ and given symbol-constellation energy E, total transmission energy is given by $\rho(\mathbf{s}) \triangleq E\|\mathbf{s}\|_2^2 = E$.

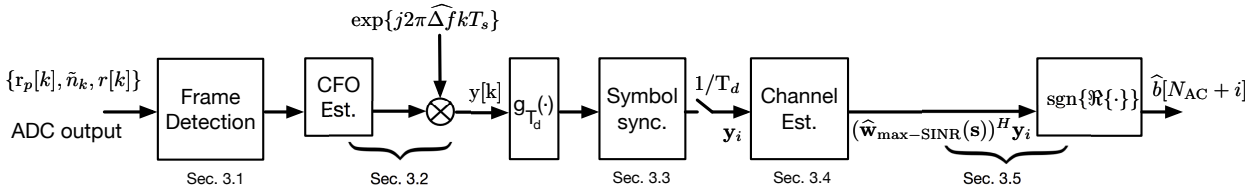

Figure 2. Receiver design.

3.4 Channel estimation

By horizontal concatenation of all J' received vectors, (14) can be written in the matrix form

$$\mathbf{Y} \triangleq \sqrt{E}\mathbf{H}\mathbf{s}\mathbf{b}^T + \widetilde{\mathbf{N}} = \mathbf{S}\mathbf{h}\mathbf{b}^T + \widetilde{\mathbf{N}} \in \mathbb{C}^{L_M \times J'} \tag{16}$$

where $\mathbf{b} \triangleq \left[b[N_{\mathrm{AC}}], \quad \ldots, \quad b[N_{\mathrm{AC}}+J'-1]\right]^T$, $\widetilde{\mathbf{N}} \triangleq \left[\tilde{\mathbf{n}}_0, \ldots, \tilde{\mathbf{n}}_{J'-1}\right]$, $\mathbf{h} \triangleq \left[\tilde{h}[0], \quad \ldots, \quad \tilde{h}[M-1]\right]^T$, and

$$\mathbf{S} \triangleq \sqrt{E}\begin{bmatrix} s_1 & & \\ \vdots & \ddots & \\ s_L & & s_1 \\ & \ddots & \vdots \\ & & s_L \end{bmatrix} \in \mathbb{R}^{L_M \times M}.$$

Then, the receiver estimates the channel coefficients $\mathbf{h}$ by using a-priori knowledge of the header symbols $\mathbf{b}_{\mathrm{HDR}} = \left[b[N_{\mathrm{AC}}], \quad \ldots, \quad b[N_{\mathrm{AC}}+N_{\mathrm{HDR}}-1]\right]^T$ and solving the least-squares (LS) problem

$$\widehat{\mathbf{h}} \triangleq \underset{\mathbf{h}\in\mathbb{C}^M}{\operatorname{argmin}} \|\mathbf{Y} - \mathbf{S}\mathbf{h}\mathbf{b}_{\mathrm{HDR}}^T\|_F^2 = \frac{1}{N_{\mathrm{HDR}}}(\mathbf{S}^H\mathbf{S})^{-1}\mathbf{S}^H\mathbf{Y}_{\mathrm{HDR}}\mathbf{b}_{\mathrm{HDR}} \tag{17}$$

where $\mathbf{Y}_{\mathrm{HDR}} \in \mathbb{C}^{L_M \times N_{\mathrm{HDR}}}$ contains the received header symbols. Accordingly, by (15) and (17), the receiver obtains an estimate $\widehat{\mathbf{H}}$ of $\mathbf{H}$.

3.5 Maximum-SINR filtering and detection

By (14), the autocorrelation matrix of the overall disturbance, $\tilde{\mathbf{n}}_i$, is $\mathbf{R}_{\tilde{\mathbf{n}}} \triangleq \mathbb{E}\{\tilde{\mathbf{n}}_i\tilde{\mathbf{n}}_i^H\} = \mathbf{R}_{\mathbf{i}} + \sigma^2\mathbf{I}_{L_M}$. The linear filter at the receiver that exhibits maximum output SINR can be found to be any scaled version of $\mathbf{w}_{\text{max-SINR}}(\mathbf{s}) \triangleq \mathbf{R}_{\tilde{\mathbf{n}}}^{-1}\mathbf{H}\mathbf{s}$. In practical applications, the disturbance autocorrelation matrix is sample-average estimated over $D > J'$ signal-absent (user of interest is silent) snapshots of the received signal as

$$\widehat{\mathbf{R}}_{\tilde{\mathbf{n}}} \triangleq \frac{1}{D}\sum_{i=0}^{D-1}\tilde{\mathbf{n}}_i\tilde{\mathbf{n}}_i^H. \tag{18}$$

Then, by (17) and (18), the estimated maximum-SINR filter takes the form $\widehat{\mathbf{w}}_{\text{max-SINR}}(\mathbf{s}) \triangleq \widehat{\mathbf{R}}_{\tilde{\mathbf{n}}}^{-1}\widehat{\mathbf{H}}\mathbf{s}$. Finally, the receiver detects the transmitted symbol $b[N_{\mathrm{AC}}+i]$, $i = 0, \ldots, J'-1$ based on the statistic $(\widehat{\mathbf{w}}_{\max-\mathrm{SINR}}(\mathbf{s}))^H\mathbf{y}_i$. For example for Binary-Phase-Shift-Keying (BPSK) constellation $\mathcal{A} = \{\pm 1\}$, the receiver detects

$$\widehat{b}[N_{\mathrm{AC}}+i] = \mathrm{sgn}(\Re\{(\widehat{\mathbf{w}}_{\max-\mathrm{SINR}}(\mathbf{s}))^H\mathbf{y}_i\}) \tag{19}$$

where $\mathrm{sgn}(\cdot)$ returns the sign of its argument (by convention, $\mathrm{sgn}(0) = 0$). The complete receiver processing chain is illustrated in Fig. 2.

4. PROPOSED SPARSE WAVEFORM DESIGN

The SINR attained at the output of $\mathbf{w}_{\max-\mathrm{SINR}}(\mathbf{s})$ is given by

$$\mathrm{SINR}(\mathbf{s}) \triangleq \frac{\mathbb{E}\{|(\mathbf{w}_{\max-\mathrm{SINR}}(\mathbf{s}))^H(\sqrt{E}\mathbf{H}\mathbf{s}b[N_{\mathrm{AC}}+i])|^2\}}{\mathbb{E}\{|(\mathbf{w}_{\max-\mathrm{SINR}}(\mathbf{s}))^H\widetilde{\mathbf{n}}_i|^2\}} = E\ \mathbf{s}^\top\mathbf{H}^H\mathbf{R}_{\tilde{\mathbf{n}}}^{-1}\mathbf{H}\mathbf{s} = E\ \mathbf{s}^\top\mathbf{P}\mathbf{s} \tag{20}$$

where $\mathbf{w}_{\text{max-SINR}}(\mathbf{s}) \triangleq \mathbf{R}_{\tilde{\mathbf{n}}}^{-1}\mathbf{H}\mathbf{s}$ and $\mathbf{P} \triangleq \mathbf{H}^H\mathbf{R}_{\tilde{\mathbf{n}}}^{-1}\mathbf{H} \succ 0$. Prior-art work[22,23] focuses on the design of a binary waveform $\mathbf{s}$ that maximizes $\mathrm{SINR}(\mathbf{s})$ at the output of the maximum-SINR filter

$$\hat{\mathbf{s}} \triangleq \underset{\mathbf{s}\in\left\{\pm\frac{1}{\sqrt{L}}\right\}^L}{\operatorname{argmax}}\ \mathrm{SINR}(\mathbf{s}) = \underset{\mathbf{s}\in\left\{\pm\frac{1}{\sqrt{L}}\right\}^L}{\operatorname{argmax}}\ \mathbf{s}^\top\mathbf{P}\mathbf{s}. \tag{21}$$

Certainly, the problem in (21) can be solved optimally by exhaustive evaluation of all 2^L binary vectors $\mathbf{s} \in \{\pm\frac{1}{\sqrt{L}}\}^L$, with cost $\mathcal{O}(2^L)$. Several reduced-cost optimal and suboptimal algorithms for the solution of (21) have also been proposed in the literature.[22–26]

In this work, we propose maximum-SINR sparse-binary waveforms. Particularly, we consider that the transmitter can adaptively select the optimal code-symbol transmission intervals to transmit and thus avoid high code-symbol-level disturbance correlations. To that end, we formulate and solve the sparse-binary waveform design problem

$$\tilde{\mathbf{s}} \triangleq \underset{\substack{\mathbf{s}\in\{0,\pm c\}^L\\ c^2\|\mathbf{s}\|_0=1,\ c\in\mathbb{R}}}{\operatorname{argmax}}\ \mathbf{s}^\top\mathbf{P}\mathbf{s}. \tag{22}$$

Notice that, similarly to (21), for every element $\mathbf{s}$ in the feasibility set of (22), $\rho(\mathbf{s}) = E\|\mathbf{s}\|_2^2 = E$, which implies

$$\rho(\tilde{\mathbf{s}}) = \rho(\hat{\mathbf{s}}). \tag{23}$$

In addition, we find that

$$\begin{aligned}\mathrm{SINR}(\tilde{\mathbf{s}}) &= \max_{\substack{\mathbf{s}\in\{0,\pm c\}^L\\ c^2\|\mathbf{s}\|_0=1,\ c\in\mathbb{R}}} \mathbf{s}^\top\mathbf{P}\mathbf{s} = \max_{K\in\{1,2,\ldots,L\}}\ \max_{\substack{\mathbf{s}\in\left\{0,\pm\frac{1}{\sqrt{K}}\right\}^L\\ \|\mathbf{s}\|_0=K}} \mathbf{s}^\top\mathbf{P}\mathbf{s} \geq \max_{K\in\{1,2,\ldots,L\}}\ \max_{\substack{\mathbf{s}\in\left\{0,\pm\frac{1}{\sqrt{K}}\right\}^L\\ \|\mathbf{s}\|_0=K}} \frac{K}{L}\ \mathbf{s}^\top\mathbf{P}\mathbf{s}\\ &= \max_{K\in\{1,2,\ldots,L\}}\ \max_{\substack{\mathbf{s}\in\left\{0,\pm\frac{1}{\sqrt{L}}\right\}^L\\ \|\mathbf{s}\|_0=K}} \mathbf{s}^\top\mathbf{P}\mathbf{s} = \max_{\mathbf{s}\in\left\{0,\pm\frac{1}{\sqrt{L}}\right\}^L} \mathbf{s}^\top\mathbf{P}\mathbf{s} \geq \max_{\mathbf{s}\in\left\{\pm\frac{1}{\sqrt{L}}\right\}^L} \mathbf{s}^\top\mathbf{P}\mathbf{s} = \mathrm{SINR}(\hat{\mathbf{s}}).\end{aligned} \tag{24}$$

By (23) and (24) we conclude that the proposed sparse-binary waveform $\tilde{\mathbf{s}}$ attains the same total transmission energy with the conventional binary waveform of (21), while at the same time offers higher or equal post-filtering SINR.

4.1 Optimal Algorithm

The problem in (22) is clearly a combinatorial problem. An optimal solution can be found by exhaustive search within its feasibility set $\{\mathbf{s} \in \{0, \pm c\}^L, c^2\|\mathbf{s}\|_0 = 1,\ c \in \mathbb{R}\}$. In the sequel, we present in detail the steps to obtain the optimal solution to (22). First we rewrite

$$\max_{\substack{\mathbf{s}\in\{0,\pm c\}^L\\ c^2\|\mathbf{s}\|_0=1,\ c\in\mathbb{R}}} \mathbf{s}^\top\mathbf{P}\mathbf{s} = \max_{K\in\{1,2,\ldots,L\}}\ \max_{\substack{\mathbf{s}\in\left\{0,\pm\frac{1}{\sqrt{K}}\right\}^L\\ \|\mathbf{s}\|_0=K}} \mathbf{s}^\top\mathbf{P}\mathbf{s}. \tag{25}$$

Optimal Algorithm

Input: $\mathbf{P} = \mathbf{H}^H \mathbf{R}_{\tilde{\mathbf{n}}}{}^{-1} \mathbf{H}$

$\tilde{\mathbf{s}} \leftarrow \frac{1}{\sqrt{L}} \mathbf{1}_L$; $m \leftarrow \tilde{\mathbf{s}}^\top \mathbf{P} \tilde{\mathbf{s}}$
for $K \in \{1, 2, \ldots, L\}$
  for $\mathcal{I} \subseteq \{1, 2, \ldots, L\}$, $|\mathcal{I}| = K$
    for $\mathbf{b} \in \{\pm \frac{1}{\sqrt{K}}\}^K$
      $[\mathbf{s}]_{\mathcal{I}} \leftarrow \mathbf{b}$, $[\mathbf{s}]_{\{1,2,\ldots,L\} \setminus \mathcal{I}} \leftarrow \mathbf{0}_{L-K}$
      if $\mathbf{s}^\top \mathbf{P} \mathbf{s} > m$, $\tilde{\mathbf{s}} \leftarrow \mathbf{s}$, $m \leftarrow \tilde{\mathbf{s}}^\top \mathbf{P} \tilde{\mathbf{s}}$

Output: $\tilde{\mathbf{s}}$

Figure 3. Pseudocode for the optimal algorithm that solves the sparse-binary waveform design problem in (22).

Then, we focus on solving the inner maximization problem in (25); i.e. for every sparsity value $K \in \{1, 2, \ldots, L\}$, we obtain

$$\tilde{\mathbf{s}}_K \stackrel{\triangle}{=} \underset{\substack{\mathbf{s} \in \left\{0, \pm \frac{1}{\sqrt{K}}\right\}^L \\ \|\mathbf{s}\|_0 = K}}{\operatorname{argmax}} \mathbf{s}^\top \mathbf{P} \mathbf{s}. \tag{26}$$

The solution to (26) can be found by examining exhaustively all $\binom{L}{K} 2^K$ elements of its feasibility set. Then, we obtain $\tilde{\mathbf{s}}$ by solving

$$\tilde{\mathbf{s}} = \underset{\mathbf{s} \in \{\tilde{\mathbf{s}}_1, \ldots, \tilde{\mathbf{s}}_L\}}{\operatorname{argmax}} \mathbf{s}^\top \mathbf{P} \mathbf{s}. \tag{27}$$

Therefore, (22) can be solved optimally with complexity $\mathcal{O}(3^L)$ by exhaustive search among all 3^L elements of its feasibility set. Figure 3 presents the pseudocode for the optimal algorithm.

4.2 Suboptimal Iterative Algorithm

The complexity of the optimal algorithm is prohibitive for real-time practical applications when L is large. Next, we present a suboptimal algorithm for solving (22) with complexity $\mathcal{O}(L^4)$. Consider decomposition of $\mathbf{P}$ –e.g., by means of eigenvalue decomposition (EVD)– as $\mathbf{P} = \mathbf{W}^H \mathbf{W}$, for some $\mathbf{W} \in \mathbb{C}^{L \times L}$. Then, by the Cauchy-Schwarz inequality,[27] we find

$$\max_{\substack{\mathbf{s} \in \left\{0, \pm \frac{1}{\sqrt{K}}\right\}^L \\ \|\mathbf{s}\|_0 = K}} \sqrt{\mathbf{s}^\top \mathbf{P} \mathbf{s}} = \max_{\substack{\mathbf{s} \in \left\{0, \pm \frac{1}{\sqrt{K}}\right\}^L \\ \|\mathbf{s}\|_0 = K}} \max_{\substack{\mathbf{a} \in \mathbb{C}^L \\ \|\mathbf{a}\|_2 = 1}} \Re\left\{\mathbf{s}^\top \mathbf{W}^H \mathbf{a}\right\} \tag{28}$$

$$= \max_{\substack{\mathbf{a} \in \mathbb{C}^L \\ \|\mathbf{a}\|_2 = 1}} \max_{\substack{\mathbf{s} \in \left\{0, \pm \frac{1}{\sqrt{K}}\right\}^L \\ \|\mathbf{s}\|_0 = K}} \Re\left\{\mathbf{s}^\top \mathbf{W}^H \mathbf{a}\right\}. \tag{29}$$

For any given $\mathbf{s}$ in the feasibility set of the outer maximization in (28), the inner maximization is achieved for

$$\mathbf{a} = \frac{\mathbf{W}\mathbf{s}}{\|\mathbf{W}\mathbf{s}\|_2}. \tag{30}$$

Also, for any $\mathbf{a}$ in the feasibility set of the outer maximization in (29), the inner maximization is achieved by

$$\mathbf{s} = \frac{1}{\sqrt{K}} \operatorname{sgn}\left(\mathcal{I}_{\mathrm{K}}\left(\Re\left\{\mathbf{W}^{\mathrm{H}} \mathbf{a}\right\}\right)\right), \tag{31}$$

where $\mathcal{I}_K(\cdot)$ returns its argument after setting to zero the $L - K$ entries with the lowest absolute values.

Suboptimal Iterative Algorithm

Input: $\mathbf{P} = \mathbf{H}^H \mathbf{R}_{\tilde{\mathbf{n}}}{}^{-1} \mathbf{H}$

calculate $\mathbf{W} \in \mathbb{C}^{L \times L}$ such that $\mathbf{P} = \mathbf{W}^H \mathbf{W}$
for $K \in \{1, 2, \ldots, L\}$
  $\mathbf{a} \leftarrow$ arbitrary in $\mathbb{C}^{L \times 1}$, with $\|\mathbf{a}\|_2 = 1$; $m \leftarrow 0$
  until convergence,
    $\mathbf{s} \leftarrow \frac{1}{\sqrt{K}} \mathrm{sgn}\left(\mathcal{I}_{\mathrm{K}}\left(\Re\left\{\mathbf{W}^{\mathrm{H}} \mathbf{a}\right\}\right)\right)$
    $\mathbf{a} \leftarrow \frac{\mathbf{W}\mathbf{s}}{\|\mathbf{W}\mathbf{s}\|_2}$
    $m' \leftarrow \mathbf{s}^\top \mathbf{P} \mathbf{s}$
    if $m' - m \leq$ threshold; $\mathbf{s}_K \leftarrow \mathbf{s}$; convergence
    $m \leftarrow m'$
$\mathbf{s}_{\mathrm{IT}} \leftarrow \mathrm{argmax}_{\mathbf{s} \in \{\mathbf{s}_1, \ldots, \mathbf{s}_L\}} \mathbf{s}^\top \mathbf{P} \mathbf{s}$

Output: $\mathbf{s}_{\mathrm{IT}}$

Figure 4. Pseudocode for the suboptimal algorithm that solves the sparse-binary waveform design problem in (22).

By the above observations, for every sparsity value $K \in \{1, 2, \ldots L\}$, the algorithm initializes at some $\mathbf{a}_K^{(0)} \in \mathbb{C}^{L \times 1}$ with $\left\|\mathbf{a}_K^{(0)}\right\|_2 = 1$ and generates a converging sequence of points in the feasibility set of (26), $\{\mathbf{s}_K^{(t)}\}_{t=1,2,\ldots}$. Specifically, at the t-th step, $t > 1$, the algorithm calculates

$$\mathbf{s}_K^{(t)} = \frac{1}{\sqrt{K}} \mathrm{sgn}\left(\mathcal{I}_{\mathrm{K}}\left(\Re\left\{\mathbf{W}^{\mathrm{H}} \mathbf{a}_{\mathrm{K}}^{(\mathrm{t}-1)}\right\}\right)\right), \tag{32}$$

$$\mathbf{a}_K^{(t)} = \frac{\mathbf{W}\mathbf{s}_K^{(t)}}{\left\|\mathbf{W}\mathbf{s}_K^{(t)}\right\|_2}. \tag{33}$$

Since $\Re\left\{\mathbf{s}_K^{(t)} \mathbf{W}^H \mathbf{a}_K^{(t)}\right\} \geq \Re\left\{\mathbf{s}_K^{(t-1)} \mathbf{W}^H \mathbf{a}_K^{(t-1)}\right\}$ and $\Re\{\mathbf{s}_K^{(t)} \mathbf{W}^H \mathbf{a}_K^{(t)}\}$ is bounded by (28), the iterations will converge in a finite number of steps $C_K > 1$. After obtaining a converging point $\mathbf{s}_K \stackrel{\triangle}{=} \mathbf{s}_K^{(C_K)}$ by the above iterations for every $K \in \{1, 2, \ldots, L\}$, the algorithm returns the approximate solution to (22)

$$\mathbf{s}_{\mathrm{IT}} \stackrel{\triangle}{=} \underset{\mathbf{s} \in \{\mathbf{s}_1, \mathbf{s}_2, \ldots, \mathbf{s}_L\}}{\mathrm{argmax}} \mathbf{s}^\top \mathbf{P} \mathbf{s}. \tag{34}$$

A complexity analysis of the presented suboptimal algorithm follows. Decomposition of matrix $\mathbf{P}$ costs $\mathcal{O}(L^3)$. Then, for every sparsity value $K \in \{1, 2, \ldots, L\}$, the algorithm executes C_K iteration steps. At each iteration step, say the t-th, the cost to find $\mathbf{s}_K^{(t)}$ and $\mathbf{a}_K^{(t)}$ is $\mathcal{O}(L^2)$. Therefore, the cost for all iterations for all values of K is $\mathcal{O}(\sum_{K=1}^{L} C_K L^2)$. Setting, in practice, $C_K \leq L$, for every K, all iterations cost $\mathcal{O}(L^4)$. Figure 4 presents the pseudocode for the suboptimal algorithm.

4.3 Waveform design from estimated statistics

As discussed in Section 3, the receiver is unaware of the exact channel matrix $\mathbf{H}$ and the disturbance autocorrelation matrix $\mathbf{R}_{\tilde{\mathbf{n}}}$. Therefore, matrix $\mathbf{P} = \mathbf{H}^H \mathbf{R}_{\tilde{\mathbf{n}}}{}^{-1} \mathbf{H}$ cannot be formulated and used for waveform design. In practice, the receiver estimates $\mathbf{P}$ as $\widehat{\mathbf{P}} \stackrel{\triangle}{=} \widehat{\mathbf{H}}^H \widehat{\mathbf{R}}_{\tilde{\mathbf{n}}}^{-1} \widehat{\mathbf{H}}$, by means of (17) and (18), and instead of (22) we seek the sparse-binary waveform that maximizes the estimated post-filtering SINR, $\widehat{\mathrm{SINR}}(\mathbf{s}) = E\, \mathbf{s}^\top \widehat{\mathbf{P}} \mathbf{s}$, as

$$\tilde{\mathbf{s}} \stackrel{\triangle}{=} \underset{\substack{\mathbf{s} \in \{0, \pm c\}^L \\ c^2 \|\mathbf{s}\|_0 = 1,\ c \in \mathbb{R}}}{\mathrm{argmax}} \mathbf{s}^\top \widehat{\mathbf{P}} \mathbf{s}. \tag{35}$$

The optimal solution to (35) is attained by the algorithm of Section 4.1, simply by substituting $\mathbf{P}$ with $\widehat{\mathbf{P}}$. Similarly, the suboptimal algorithm of Section 4.2 is also straightforwardly applicable to (35).

5. EXPERIMENTAL RESULTS

In this section, we first present simulation studies of both the optimal and the suboptimal algorithms for designing maximum-SINR sparse-binary waveforms. Then, the post-filtering SINR and BER performance attained by the proposed sparse-binary waveforms is experimentally verified in a SDR testbed of a SISO communication system operating in a multipath laboratory environment, in the presence of colored interference.

In the simulation studies, we fix $L = 13$, $M = 1$, $\mathbf{R_i}$ such that $\mathrm{Tr}(\mathbf{R_i}) = 10$ dB, $\mathbf{H}$ such that $\|\mathbf{H}\|_F = 1$, $\sigma = 1$, and $E = 10$ dB. Figure 5 depicts the post-filtering SINR attained by the solution of (26), $\tilde{\mathbf{s}}_K$, versus different sparsity values $K = 1, \ldots, L$. We compare the SINR performance of $\tilde{\mathbf{s}}_K$, with the solution to the binary waveform optimization problem in (21), $\hat{\mathbf{s}}$, and the optimal sparse-binary waveform $\tilde{\mathbf{s}}$ that solves (22). As expected, we observe that $\mathrm{SINR}(\hat{\mathbf{s}}) = \mathrm{SINR}(\tilde{\mathbf{s}}_L)$. For sparsity K varying from 4 to 12, $\tilde{\mathbf{s}}_K$ outperforms $\hat{\mathbf{s}}$ with a maximum SINR difference for $K = 8$ (i.e. $\tilde{\mathbf{s}} = \tilde{\mathbf{s}}_8$). Thus, Fig. 5 verifies our theoretical results in Section 4.

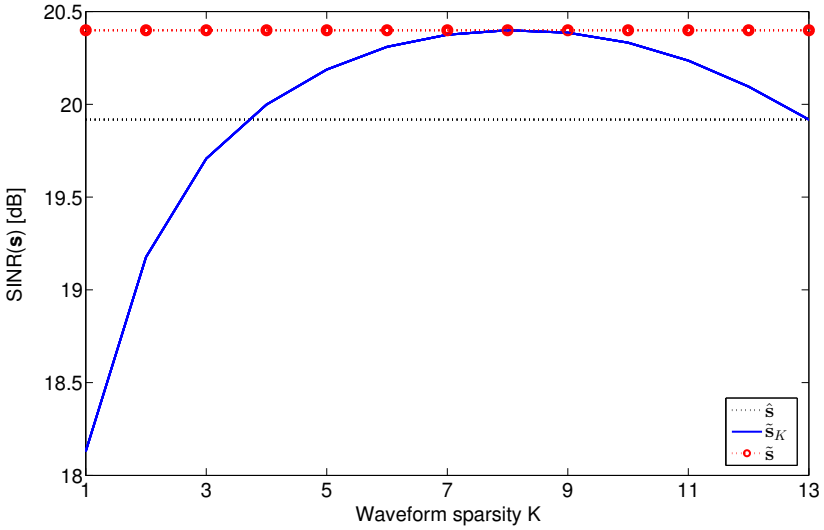

Figure 5. Maximum post-filtering SINR versus sparsity K.

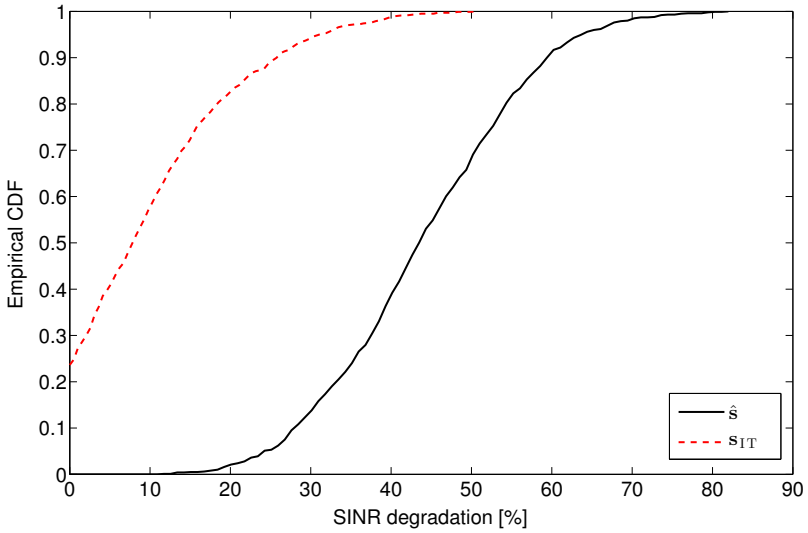

Figure 6. Empirical CDF of performance degradation attained by $\hat{\mathbf{s}}$ and $\mathbf{s}_{\mathrm{IT}}$ with respect to the proposed optimal sparse-binary waveform $\tilde{\mathbf{s}}$.

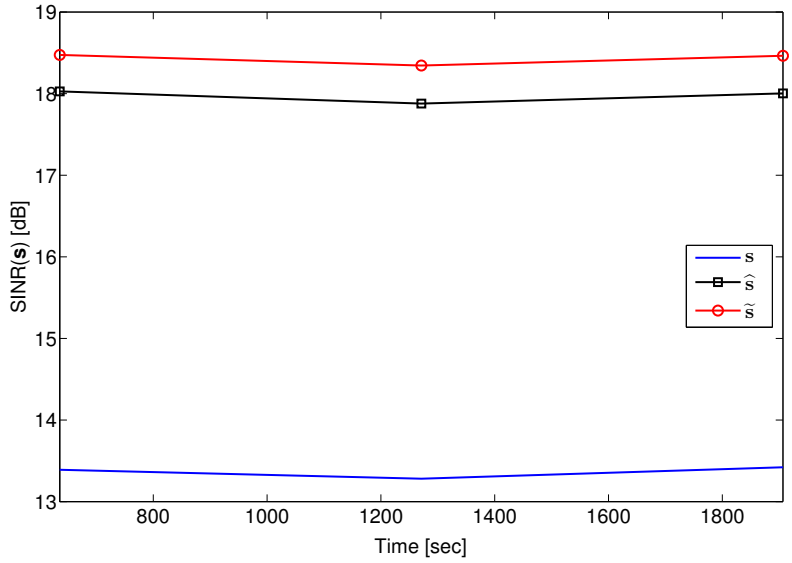

(a)

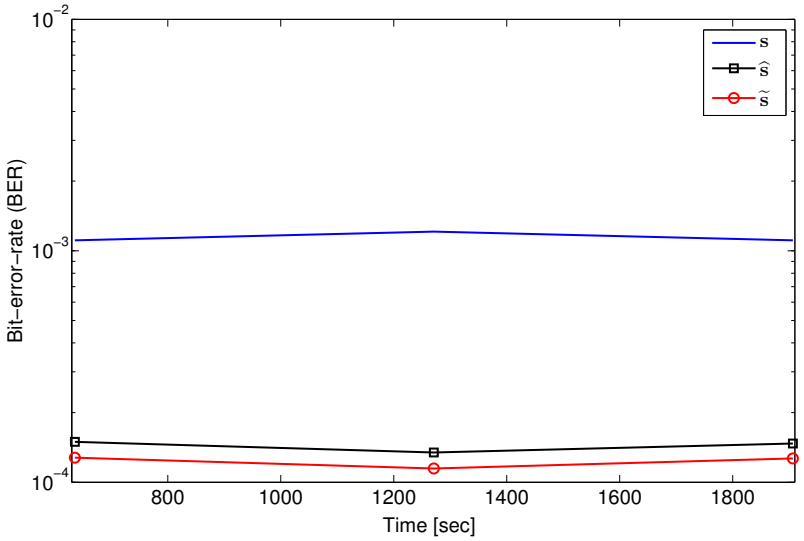

(b)

Figure 7. (a) Post-filtering SINR and (b) BER performance attained by an arbitrarily selected waveform $\mathbf{s}$, the binary optimal waveform $\hat{\mathbf{s}}$, and the proposed optimal sparse-binary waveform $\tilde{\mathbf{s}}$ in the SDR testbed.

Figure 6 presents the empirical cumulative distribution function (CDF) of the SINR performance degradation percentage attained by the optimal non-sparse binary waveform $\hat{\mathbf{s}}$ and the sparse-binary waveform $\mathbf{s}_{\rm IT}$ (calculated by the proposed suboptimal algorithm) with respect to the optimal sparse-binary waveform $\tilde{\mathbf{s}}$. The SINR degradation percentage is defined as $\frac{\mathrm{SINR}(\tilde{\mathbf{s}})-\mathrm{SINR}(\mathbf{s})}{\mathrm{SINR}(\tilde{\mathbf{s}})}\%$, where $\mathbf{s}$ is any waveform with $\|\mathbf{s}\|_2 = 1$. The CDF is calculated over 1000 independent channel realizations and disturbance autocorrelation matrices $\mathbf{R_i} \succ 0$ with $\mathrm{Tr}(\mathbf{R_i}) = 10$ dB and $\sigma = 1$. We observe that $\hat{\mathbf{s}}$ attains at least 15% lower SINR than $\tilde{\mathbf{s}}$ and SINR degradation can be as high as 80%. On the other hand, SINR degradation for the sparse-binary waveform $\mathbf{s}_{\rm IT}$ is no more than 50% with empirical probability 1. Finally, the sparse-binary waveform $\mathbf{s}_{\rm IT}$ is equivalent to $\tilde{\mathbf{s}}$ (i.e. SINR degradation is 0) with empirical probability 0.25.

Next, we evaluate experimentally the performance of the proposed sparse-binary waveform design in an indoor SDR testbed setup. In particular, the testbed comprises a pair of USRP − N210s that operate at $f_c = 2.485\,\text{GHz}$ in the presence of colored interference. Interference is generated by a different USRP − N210 that operates at the same time and frequency with the user of interest. All three USRP − N210s are interfaced with SBX daughtercards that support broadband operation from 400 MHz to 4.4 GHz. Transmission energy is fixed to be equal for both the user of interest and the interferer. We consider BPSK frame transmissions of length $J = 768$ symbols that are modulated by arbitrary all-spectrum binary waveforms of length $L = 13$. Sampling period is set to $T_s = 1\,\mu\text{s}$ and we select $I = 4$ samples per code-symbol, thus $T_d = 4\,\mu\text{s}$. A Barker sequence of length $N_{\text{P}} = 13$ is used as a preamble for frame detection, $N_{\text{AC}} = 128$ unmodulated bits are considered for frequency synchronization, and $N_{\text{HDR}} = 32$ symbols are used for symbol-level time synchronization and channel estimation. In addition, we consider a pause interval of 0.8 ms between the preamble and the access code, while burst frame transmissions are separated by silent intervals of 50 ms. The number of channel paths is considered to be $M = 2$ and SRRC pulse-shaping filters use $\alpha = 0.35$ roll-off factor.

Figure 7 depicts the post-filtering SINR and BER performance of the user of interest for an arbitrarily selected waveform $\mathbf{s}$, an optimal non-sparse binary waveform $\hat{\mathbf{s}}$, and the proposed optimal sparse-binary waveform $\tilde{\mathbf{s}}$. More specifically, waveform $\mathbf{s}$ is arbitrarily set equal to $\frac{1}{\sqrt{13}}\Big[-1,-1,+1,+1,+1,-1,-1,-1,+1,+1,+1,+1,-1\Big]^T$. The optimal binary waveform that maximizes the estimated SINR at the output of the maximum-SINR filter is found to be $\hat{\mathbf{s}} = \frac{1}{\sqrt{13}}\Big[-1,+1,-1,+1,-1,+1,-1,+1,-1,+1,-1,+1,-1\Big]^T$ and the proposed sparse-binary waveform is $\tilde{\mathbf{s}} = \frac{1}{\sqrt{10}}\Big[0,0,+1,-1,+1,-1,+1,-1,+1,-1,+1,-1,0\Big]^T$. Each data point in Fig. 7 is the result of experimental SINR and BER measurements that are averaged over a time window of 7000 frames (which corresponds to a duration of $\sim$ 635 sec). We observe that the proposed optimal sparse-binary waveform $\tilde{\mathbf{s}}$ offers 38% SINR performance improvement with respect to the arbitrarily selected binary waveform $\mathbf{s}$. Importantly, the non-sparse binary waveform $\hat{\mathbf{s}}$ offers 34% SINR performance improvement. Superior performance of the proposed sparse-binary waveform is also evident in our BER experimental results. The benefits of sparsity ($K = 10$ for these experiments) are clearly shown in practice for the first time and are in accordance with our simulation and theoretical results.

6. CONCLUSIONS

We considered the design of maximum-SINR sparse-binary waveforms and presented an optimal waveform design algorithm. In pursuit of a computationally efficient solution we also presented a suboptimal algorithm with significantly lower computational cost. In addition, we addressed receiver design considerations to experimentally evaluate the SINR and BER performance of the proposed sparse-binary waveforms in a SDR testbed. Both numerical and experimental studies demonstrated the superior SINR and BER performance of sparse-binary waveforms when compared to conventional non-sparse counterparts.

REFERENCES

[1] Li, M., Kundu, S., Pados, D. A., and Batalama, S. N., "Waveform design for secure siso transmissions and multicasting," *IEEE J. Sel. Areas Commun.* **31**, 1864–1874 (Sep. 2013).

[2] Li, M., Kundu, S., Pados, D. A., and Batalama, S. N., "Secure waveforms for siso channels," in [*Proc. IEEE Int. Conf. Acoust. Speech Signal Process. (ICASSP),* Vancouver, BC], 4713–4717 (May 2013).

[3] Wei, L., Pados, D. A., Batalama, S. N., Medley, M. J., and Hu, R. Q., "Advances in multiuser data embedding in digital media: Orthogonal sum-sinr-optimal carriers," in [*Proc. IEEE Int. Conf. Commun. (ICC),* Sydney, Australia], 963–968 (Jun. 2014).

[4] Li, M., Kulhandjian, M. K., Pados, D. A., Batalama, S. N., and Medley, M. J., "Extracting spread-spectrum hidden data from digital media," *IEEE Trans. Inf. Forensics Security* **8**, 1201–1210 (Jul. 2013).

[5] Gkizeli, M., Pados, D. A., and Medley, M. J., "Optimal signature design for spread-spectrum steganography," *IEEE Trans. Image Process.* **16**, 391–405 (Feb. 2007).

[6] Gkizeli, M., Pados, D. A., Batalama, S. N., and Medley, M. J., "Blind iterative recovery of spread-spectrum steganographic messages," in [*IEEE Int. Conf on Image Process. (ICIP),* Genova, Italy], **2**, II–1098–101 (Sep. 2005).
[7] Gao, K., Batalama, S. N., Pados, D. A., and Matyjas, J. D., "Cognitive code-division channelization," *IEEE Trans. Wireless Commun.* **10**, 1090–1097 (Apr. 2011).
[8] Gao, K., Batalama, S. N., Pados, D. A., and Matyjas, J. D., "Cognitive CDMA channelization," in [*Proc. IEEE Asilomar Conf. Signals, Syst. and Comput.,* Pacific Grove, CA], 672–676 (Nov. 2009).
[9] Sklivanitis, G., Demirors, E., Gannon, A. M., Batalama, S. N., Pados, D. A., and Melodia, T., "All-spectrum cognitive channelization around narrowband and wideband primary stations," in [*Proc. IEEE Global Commun. Conf. (GLOBECOM),* San Diego, CA], 1–7 (Dec. 2015).
[10] Sklivanitis, G., Demirors, E., Batalama, S. N., Pados, D. A., and Melodia, T., "ROCH: Software-defined radio toolbox for experimental evaluation of all-spectrum cognitive networking," in [*Proc. ACM Workshop Software Radio Implem. Forum (SRIF),* Paris, France], 10–10 (Sep. 2015).
[11] Sklivanitis, G., Demirors, E., Batalama, S. N., Pados, D. A., and Melodia, T., "Realizing all-spectrum cognitive networking on a software-defined radio testbed," in [*Proc. ACM Workshop Wireless S3,* Paris, France], 18–18 (Sep. 2015).
[12] Sklivanitis, G., Demirors, E., Batalama, S. N., Melodia, T., and Pados, D. A., "Receiver configuration and testbed development for underwater cognitive channelization," in [*Proc. IEEE Asilomar Conf. on Signals, Syst. and Comput.*], 1594–1598 (Nov. 2014).
[13] Beek, J. V. D. and Popovic, B. M., "Multiple access with low-density signatures," in [*Proc. IEEE Global Commun. Conf. (GLOBECOM),* Honolulu, HI], 1–6 (Nov. 2009).
[14] Yoshida, M. and Tanaka, T., "Analysis of sparsely-spread CDMA via statistical mechanics," in [*Proc. IEEE Int. Symp. Inf. Theory (ISIT),* Seattle, WA], 2378–2382 (Jul. 2006).
[15] Guo, D. and Wang, C., "Multiuser detection of sparsely spread cdma," *IEEE J. Sel. Areas Commun.* **26**, 421–431 (Apr. 2008).
[16] Hoshyar, R., Wathan, F. P., and Tafazolli, R., "Novel low-density signature for synchronous cdma systems over AWGN channel," *IEEE Trans. Signal Process.* **56**, 1616–1626 (Apr. 2008).
[17] Nikopour, H. and Baligh, H., "Sparse code multiple access," in [*Proc. IEEE Ann. Int. Symp. Personal, Indoor, and Mobile Radio Commun. (PIMRC),* London, UK], 332–336 (Sep. 2013).
[18] Karystinos, G. N. and Pados, D. A., "New bounds on the total squared correlation and optimum design of ds-cdma binary signature sets," *IEEE Trans. Commun.* **51**, 48–51 (Jan. 2003).
[19] Li, M., Batalama, S. N., Pados, D. A., and Matyjas, J. D., "New bounds on the total-squared-correlation of quaternary signature sets and optimal designs," in [*Proc. IEEE Global Commun. Conf. (GLOBECOM),* Honolulu, HI], 1–5 (Nov. 2009).
[20] Song, G., Wang, X., and Cheng, J., "Signature design of sparsely spread CDMA based on superposed constellation distance analysis," *CoRR* **abs/1604.04362** (2016).
[21] Ganapathy, H., Pados, D. A., and Karystinos, G. N., "New bounds and optimal binary signature sets - part ii: Aperiodic total squared correlation," *IEEE Trans. Commun.* **59**, 1411–1420 (May 2011).
[22] Karystinos, G. N. and Pados, D. A., "Rank-2-optimal adaptive design of binary spreading codes," *IEEE Trans. Inf. Theory* **53**, 3075–3080 (Sep. 2007).
[23] Karystinos, G. N. and Liavas, A. P., "Efficient computation of the binary vector that maximizes a rank-deficient quadratic form," *IEEE Trans. Inf. Theory* **56**, 3581–3593 (Jul. 2010).
[24] Kundu, S., Markopoulos, P. P., and Pados, D. A., "Fast computation of the L1-principal component of real-valued data," in [*Proc. IEEE Int. Conf. Acoust. Speech Signal Process. (ICASSP),* Florence, Italy], 8028–8032 (May 2014).
[25] Markopoulos, P. P., Karystinos, G. N., and Pados, D. A., "Optimal algorithms for L1-subspace signal processing," *IEEE Trans. Signal Process.* **62**, 5046–5058 (Oct. 2014).
[26] Markopoulos, P. P., "Reduced-rank filtering on L1-norm subspaces," in [*Proc. IEEE Sensor Array Multichannel Signal Process. Workshop (SAM),* Rio de Janeiro, Brazil], 1–5 (Jul. 2016).
[27] Golub, G. H. and Van Loan, C. F., [*Matrix Computations (3rd Ed.)*], Johns Hopkins University Press, Baltimore, MD (1996).